Optimization of Combined Radiation and Gold Nanoparticle Hyperthermia Therapy for Treating Cutaneous Squamous Carcinoma

BEE 4530
Computer Aided Engineering: Applications to Biomedical Processes

Sitara Sankar
Michelle Zhang

May 4, 2015

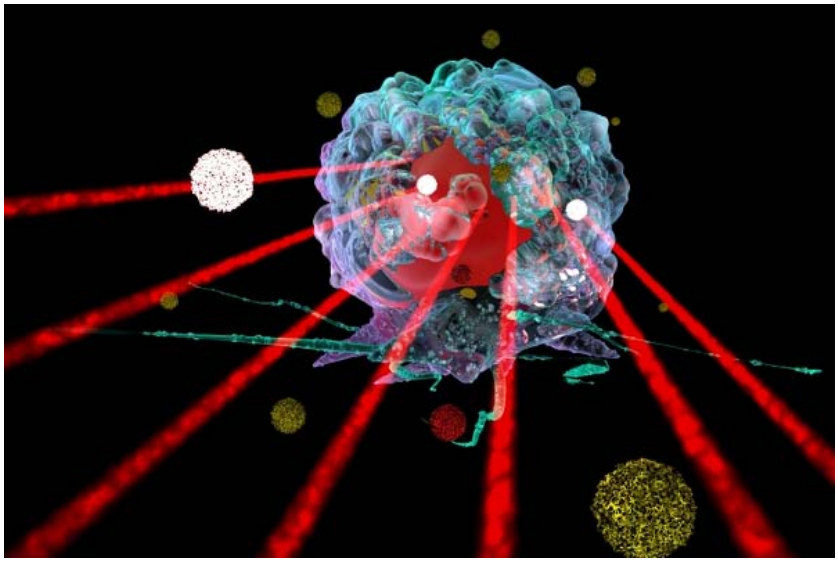

[1]

Contents

I. Executive Summary

Radiation therapy offers the ability to kill and shrink tumors non-invasively and serves as adjuvant therapy post-surgery and as primary therapy for patients unable to undergo surgery. But the process is nonspecific and nearby healthy tissue exposed to the radiation can also undergo the same ablation process that kills tumor cells. A possible solution is coupling the radiation therapy with directed hyperthermia. Tumors exposed to elevated temperatures of 40-45°C during hyperthermia exhibit increased sensitivity to radiation therapy and are more likely undergo ablation. The heating process of the tissue can be controlled by directly injecting the tumor with gold nanoparticles (AuNPs), which can absorb near infrared light and heat the tumor faster. This project models the treatment of subcutaneous squamous carcinoma using AuNP controlled hyperthermia and X-ray radiation therapy.

Using COMSOL Multiphysics 4.3b using 2D axisymmetric coordinates, we simplified the geometry of the tumor and surrounding tissue. We modeled two overall processes vital to the treatment: diffusion of AuNPs injected into the tumor and the heating process of hyperthermia-radiation therapy. We optimized the heating and radiation dosage combination for maximized tumor death and minimized tissue damage. Survival fraction of tumor and tissue were evaluated using a linear quadratic model of radiation dosage modified for thermal treatments.

Our model shows the results for AuNPs diffusion and hyperthermia-radiation tissue ablation. The optimized combination of hyperthermia and X-ray dosage was determined to be 60 seconds of heating using a 1.5 W/cm^2 infrared lamp and 0.35 Gy. This hyperthermia and radiation dosage model takes advantage of AuNP's ability to increase tumor sensitivity to radiation therapy. By optimizing the heating time and radiation dosage combination, we can reduce the total radiation exposure and the length of treatment, allowing for overall faster and less harmful treatments for patients.

II. Introduction

Nonmelanoma skin cancer is the most common cancer in the United States with approximately one million new cases reported every year. Approximately 20% of the cases are cutaneous squamous cell carcinoma (SCC) [2]. Unlike its more common basal cell carcinoma counterpart, SCC is more aggressive. This type of cancer has the ability to metastasize and penetrate other organs throughout the body, making management and treatment of SCC at the earlier stages of great interest [3].

Radiation therapy, which involves the exposure of cancer cells to high energy waves, continues to be a conventional cancer treatment due to its potency in cancer cell destruction and tumor shrinkage [2]. While radiotherapy is efficient, it frequently cannot be delivered at the ideal curative dosage because of the damage it will instill to surrounding, healthy tissue [2]. High radiation dosages also result in numerous unfavorable side effects for the patient [2]. Hyperthermia, the heating of tissues to elevated temperatures, usually 40°C - 45°C, is being studied as a radiosensitization mechanism, meant to increase the sensitivity of cancer cells to radiation and thereby reduce the curative radiation dosage [4]. Hyperthermia has been shown to be multifunctional in radiosensitization. Hyperthermia causes direct cytotoxicity to cells and additionally interferes with tumor blood flow and oxygenation, thus weakening cells and increasing post-radiation death [5].

Clinical studies have indicated improved radiotherapy responses after hyperthermia treatment in breast, neck, skin, and brain cancers [5]. One important study has shown that when hyperthermia and radiation are applied simultaneously, a high thermal enhancement ratio (radiation dose for radiation only divided by radiation dose for radiation post hyperthermia) of up to 8:1 can be achieved [2]. Although trials show promising potential for combined hyperthermia-radiation treatment, utilization of this technique is still limited. This is largely due to the lack of dosimetric data for this treatment approach, inhibiting physicians from unambiguously prescribing hyperthermia and radiation dosages [5]. Hyperthermia-radiation treatment is also limited by its inability to penetrate deep tumors without overheating surrounding tissues [2].

There has recently been a technological development in the field of cancer therapeutics: gold nanoparticle (AuNP) mediated hyperthermia. This therapy is said to have enhanced efficacy, decreased invasiveness, and fewer side effects than other popular forms of cancer therapy [6]. Gold-nanoparticles function to increase absorption. The nanoparticles, when exposed to light at their resonance wavelength, generate a synchronized oscillation, resulting in light scattering or absorption, which can be optimized for therapeutic applications [6]. For tumor treatment, nanoparticles are injected straight into the tumor [6]. The tumor is then exposed to an infrared heating source, absorbs the energy, and heats and kills the tumor cells [6].

Preclinical studies indicate that the extent of hyperthermia radiosensitization depends on the duration and temperature achieved during hyperthermia, but precise quantification is still lacking [5]. Contributions to addressing this gap were made by Kok et al, who through experimentation, developed a numerical method to convert radiations dosages without hyperthermia to equivalent radiation doses with hyperthermia [4]. Utilizing this numerical method after modeling the heat transfer process during gold nanoparticle mediated hyperthermia will allow for the determination of average tumor and healthy tissue temperatures for various hyperthermia durations, followed by the determination of corresponding radiation dosages. Such a model will enable the optimization of hyperthermia length and radiation dosage in order to maximize tumor cell death while minimizing cell death of surrounding tissue.

A. Problem Statement

AuNP is currently only assumed to have even distribution within the tumor after 24 hours, adding to the ambiguity in the treatment process. Furthermore, clinical use of consecutive hyperthermia and radiotherapy treatments is currently limited because of unclear dosimetry for the combination of hyperthermia and radiotherapy treatment.

B. Design Objectives

We propose to model the diffusion of AuNP in the tumor to propose a viable time-frame for hyperthermia-radiation treatment after the initial AuNP injection. We will also model the effects of hyperthermia on radiation therapy to determine the optimal heating time length and radiation dosage combination. To do this, we have the following design objectives:

1. Model the 2D axisymmetric AuNP injection and diffusion throughout the SCC tumor to propose a viable time frame for hyperthermia-radiation treatment post-injection.
2. Model the 2D axisymmetric heat transfer process associated with using an infrared heating lamp to apply hyperthermia therapy to a SCC tumor for a range of heating times.
3. Quantify average tumor temperature and average surrounding tissue temperature for different hyperthermia durations and utilize a numerical method to calculate corresponding radiation dosage and cell survival fraction for each duration.
4. Optimize hyperthermia time, radiation dosage, and survival fraction such that survival fraction of the tumor cells is minimized, survival fraction of the surrounding tissue is maximized, and radiation dosage is minimized.

C. Schematics

Squamous cell carcinoma (SCC) hyperthermia and radiation therapy process is simulated with a simplified 2D axisymmetric model. The spherical tumor is 1 mm underneath the skin surface -- directly under the avascularized epidermis layer. Part of the tumor is in contact with the vascularized dermis layer. The carcinoma is epiphytic and protrudes 3mm above the skin surface. The schematic for the first module in our model, AuNP diffusion, is shown in Figure 1 below and schematic for the second module in our model, hyperthermia heating, is shown in Figure 2 below. Governing equations, boundary equations, and initial equations for both modules are found in Appendix A. Our third module, radiation therapy, was not modeled using COMSOL, but the linear quadratic equations modeling the effects of tumor ablation are also found in Appendix A.

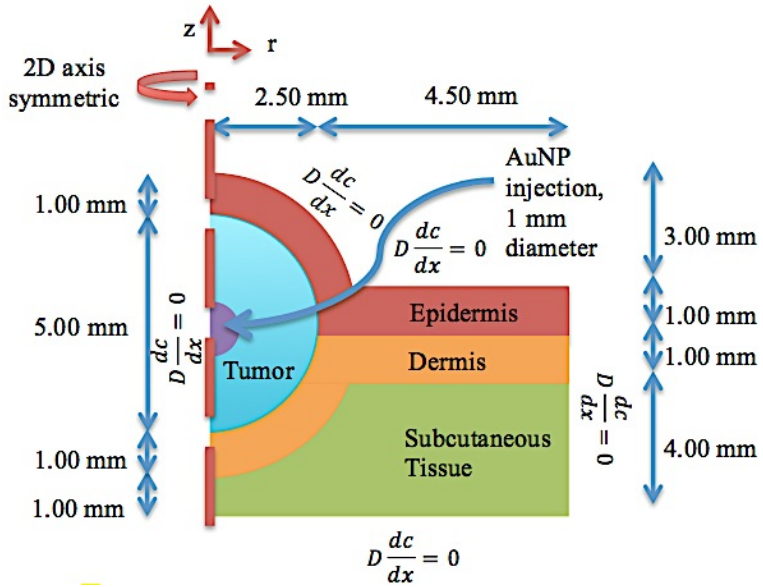

Figure 1. Schematic for modeling the diffusion of AuNPs (Module 1). SCC was modeled as a spherical tumor located 1 mm below the epidermal surface. The tumor is epiphytic with a protrusion of 3 mm above the skin. 100 uL of AuNP (100 mg/mL) is injected at the center of the tumor. More information regarding the governing equations, boundary equations, and initial conditions are found in Appendix A.

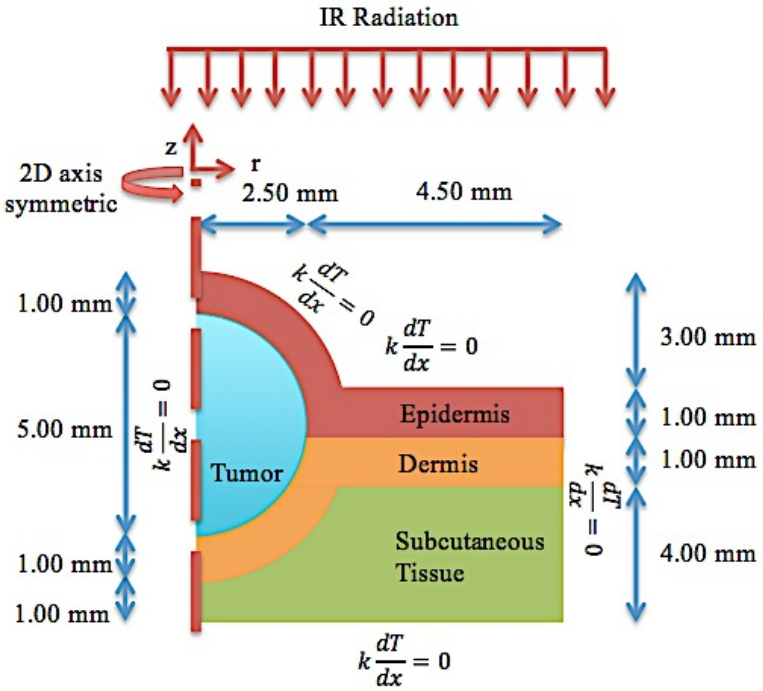

Figure 2. Schematic for modeling hyperthermia (Module 2). SCC was modeled as a spherical tumor located 1 mm below the epidermal surface. The tumor is epiphytic with a protrusion of 3 mm above the skin. 1.5W/cm^2 infrared lamp is shining perpendicular to the skin. More information regarding the governing equations, boundary equations, and initial conditions are found in Appendix A.

III. Results

Module 1 -- AuNP Diffusion

2D axisymmetric AuNP injection and diffusion throughout the SCC tumor was modeled. The results show that the AuNPs are relatively evenly distributed throughout the tumor after 24 hours, as the experimental papers have assumed, but this concentration profile is very sensitive to the diffusivity of the nanoparticle in the healthy tissue. It was found that within our range of certainty of the value for nanoparticle diffusivity in the tumor, a full 24 hours was not needed for even distribution of the nanoparticle. A 24 hour diffusion time results in some of the nanoparticle seeping into the surrounding tissue. An optimal diffusion time of 6.4 hours was determined. Details about mesh convergences can be found in Appendix B.

Sensitivity Analysis

A sensitivity analysis was done for the two diffusivity coefficients: the diffusivity of the nanoparticle in the tumor and the diffusivity of nanoparticle in the healthy tissue. These parameters were chosen for sensitivity analysis because exact values for these parameters were not found. Rather, these parameters were estimated based on parameters given for similar molecules. The diffusivity of the nanoparticle in healthy tissue was varied over a much wider range than the diffusivity of the nanoparticle in the tumor because the accuracy of the parameter greater uncertainty than the accuracy of the value used. As seen in Figure 3, there is little variability in nanoparticle concentration values over our estimated range of uncertainty for the diffusivity of nanoparticle in the tumor.

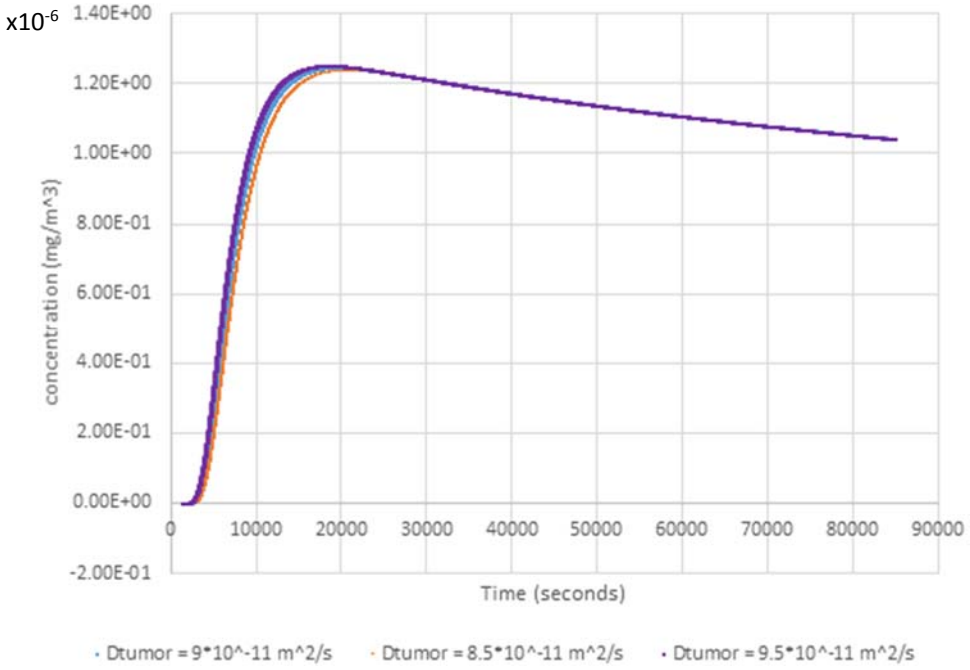

Figure 3. Sensitivity analysis for varying diffusivity of AuNPs in tumor. There is low variability in the concentration of AuNPs from varying the diffusivity of AuNPs in the tumor.

There is significantly more variability in nanoparticle concentration values over our estimated range of uncertainty for the diffusivity of nanoparticle in the healthy tissue, as seen in Figure 4 below.

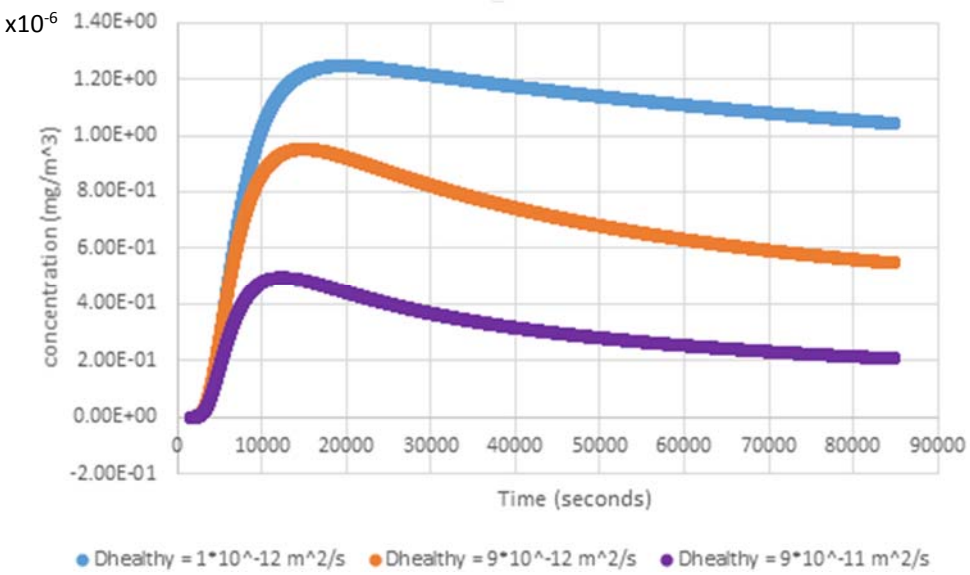

Figure 4. Sensitivity analysis for varying diffusivity of AuNPs in healthy tissue. There is an noticeable difference in the concentration of AuNPs in the tumor from varying the diffusivity of AuNPs in the tissue.

The effect of this large variability is seen in the surface plots in Figure 5, which depict the concentration profile after 24 hours of nanoparticle diffusion. When the diffusivity is $1*10^{-12}$ m^2/s, the concentration profile is as expected. Namely, the nanoparticle is concentrated evenly within the tumor and diffuses very slightly into the outside healthy tissue. When the diffusivity is $9*10^{-12}$ m^2/s, the nanoparticle is distributed evenly within the tumor, but there is a greater leakage of nanoparticle into the surrounding healthy tissue. When the diffusivity is $9*10^{-11}$ m^2/s, which is the same as the diffusivity of nanoparticle in the tumor, it appears that a significant amount of nanoparticles have leaked into the surrounding healthy tissue.

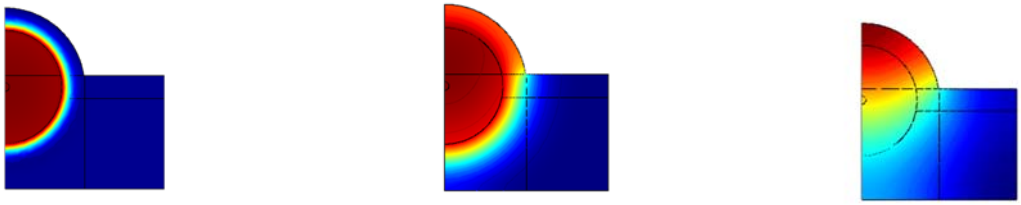

A. D = $1*10^{-12}$ m^2/s B. D = $9*10^{-12}$ m^2/s C. D = $9*10^{-11}$ m^2/s

Figure 5. 2D concentration profiles of geometry where diffusivity of AuNP in tumor is $1*10^{-12}$ m^2/s (A), $9*10^{-12}$ m^2/s (B), and $9*10^{-11}$ m^2/s (C). At lower diffusivities, nanoparticles are more concentrated in the tumor.

This sensitivity analysis reveals that our uncertainty in the diffusivity of the nanoparticle in the healthy tissue has significant repercussions, while our level of certainty in the diffusivity of nanoparticle in the tumor region is adequate. We found that the diffusion profile only behaves as expected if the diffusivity of nanoparticle in the healthy tissue is at least an order of magnitude lower than the diffusivity of nanoparticle in the tumor. However, by viewing the animation of the diffusion process, we were able to suggest a better diffusion time for the case where both diffusivities are close in value and on the same order of magnitude.

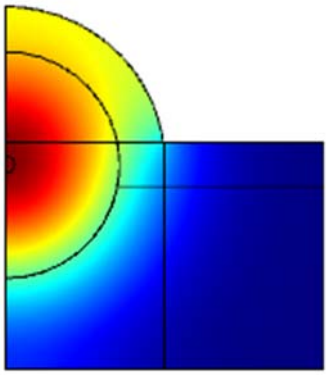

$D = 9*10^{-11}$ m^2/s, t = 6.4 hours

Figure 6. 2D concentration profiles of geometry where diffusivity of AuNP in tumor is $9*10^{-11}$ m^2/s at 6.4 hours after injection. Most of the AuNPs are still within the tumor and have not diffused into the healthy surrounding tissue.

Figure 6 shows a concentration profile for the case where both diffusivities are $9*10^{-11}$ m^2/s, but the diffusion time is only 6.4 hours instead of 24 hours. While the concentration profile is still not as ideal as in Figures 5a or 5b above, the concentration profile is more uniform that in Figure 5c above.

Using AuNP-tumor diffusivity and AuNP-tissue diffusivity as shown in the parameters table, our AuNP diffusion model successfully showed that AuNPs was evenly distributed throughout the tumor after 24 hours, but that there was likely some degree of diffusion into the healthy tissue at this time. We analyzed the sensitivity of these predicted diffusivities and showed that the ideal scenario with an evenly distributed concentration profile within the tumor and a minimal AuNP leakage into healthy tissue occurred at times well below 24 hours post-injection even with ambiguity in our proposed diffusivity parameters. We propose an optimal AuNP diffusion time of 6.4 hours.

Module 2 and 3 – Hyperthermia-Radiation Treatment

2D axisymmetric hyperthermia process was modeled with the assumption that infrared absorption only depended on penetration depth. This assumption was supported by the AuNP-diffusion model: AuNPs have an even concentration profile by the time hyperthermia starts, so only penetration depth for infrared spectrum in tissue affected the degree in which electromagnetic energy is converted into thermal energy. Details regarding governing equations, boundary equations, and initial conditions are found in Appendix A. Average temperatures of the skin and of the tumor were computed. The results are shown in Figure 7.

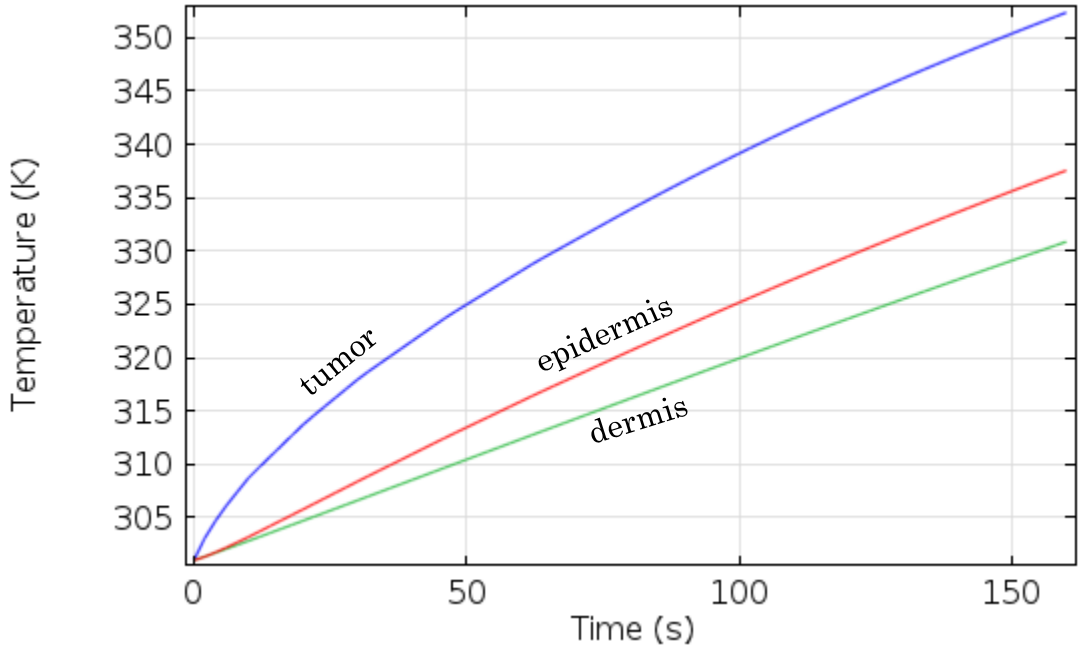

Figure 7. Average temperatures of tumor, dermis, and epidermis. After 60 seconds of heating with a 1.5W/cm^2 infrared lamp, the epidermis reaches 43°C, which is the temperature where most tissue becomes irreversibly damaged.

After 60 seconds of heating with a 1.5W/cm^2 infrared lamp, the epidermis reaches 43°C, which is the temperature where most tissue becomes irreversibly damaged. Therefore, we added a time constraint to our hyperthermia-radiation coupling step: the maximum time length of heating is 60 seconds.

Using the modeled average temperatures, we determined survival fractions using equations found in Module 3 in Appendix A. A parametric sweep for varying dosages were created and used to analyze the extent of tissue damage in the hyperthermia-radiation treatment process. The ideal hyperthermia heating and radiation dosage combination was determined using an optimization function and the robustness of the results was probed using a sensitivity analysis.

Optimization Function

To identify the combination of hyperthermia and dosage that results in the best treatment result in our model, we proposed an optimization function that accounts for the ablation of tumor cells, the survival of the surrounding healthy tissue, and the patient's exposure to radiation. There's no doubt that the best treatment would have all the tumors gone and none of the healthy tissues damaged while the patient receives no dosage exposure – the tumor simply disappears. And the worst treatment would have all the opposite effects. This idea is reflected by the proposed optimization function (Eq. 1) that gives respective weights to the survival fraction of the tumor, the survival fraction of healthy tissue, and radiation dosage.

$$J = \sum_i F_{Tumor}(SF_i) + \sum_i F_{Tissue}(SF_i) + \sum_i F_{Radiation}(d_i) \qquad \text{(Eq. 1)}$$

$$F_{Tumor}(SF) = \begin{cases} 230, & 0 < SF \leq 0.05 \\ 200, & 0.05 < SF \leq 0.10 \\ 10, & 0.10 < SF \leq 0.50 \\ 0, & 0.50 < SF \leq 1.0 \end{cases}$$

$$F_{\square issue}(SF) = \begin{cases} 0, & 0 < SF \leq 0.60 \\ 20, & 0.60 < SF \leq 0.80 \\ 90, & 0.80 < SF \leq 0.90 \\ 120, & 0.90 < SF \leq 1.0 \end{cases}$$

$$F_{Radiation}(d) = \begin{cases} 60, & 0\ Gy < R \leq 0.5\ Gy \\ 30, & 0.5\ Gy < R \leq 1.0\ Gy \\ 15, & 1.5\ Gy < R \leq 1.0\ Gy \\ 0, & R > 1.5\ Gy \end{cases}$$

Four optimization functions were plotted for varying hyperthermia treatment time (0, 20, 40, 60 seconds) and are shown in Figure 8 below.

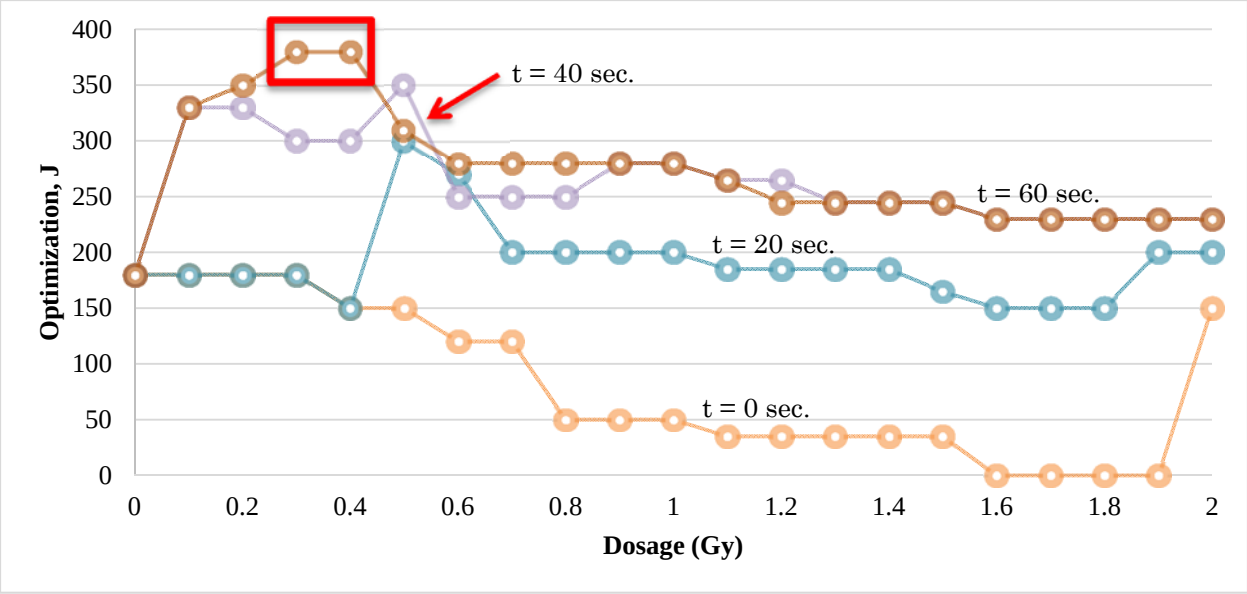

Figure 8. Optimization function for determining optimal dosage-time combination for AuNP-hyperthermia-radiation therapy. Based on the optimization function proposed, the larger the J value, the more favorable outcome the therapy is predicted to be. The recommended dosage shows that the optimal combination for AuNP-hyperthermia-radiation therapy for our model is 60 seconds of infrared radiation with a 1.5 W/cm^2 lamp followed by 0.35 Gy of radiation therapy.

The more favorable outcome has a larger J value. The function shows a maximum peak at 60 seconds at approximately 0.35 Gy, and is therefore our recommended dosage for this model. We modeled the temperature profile and the survival fraction profile of the tumor and healthy tissue for this recommended treatment and the results are shown in shown in Figure 9.

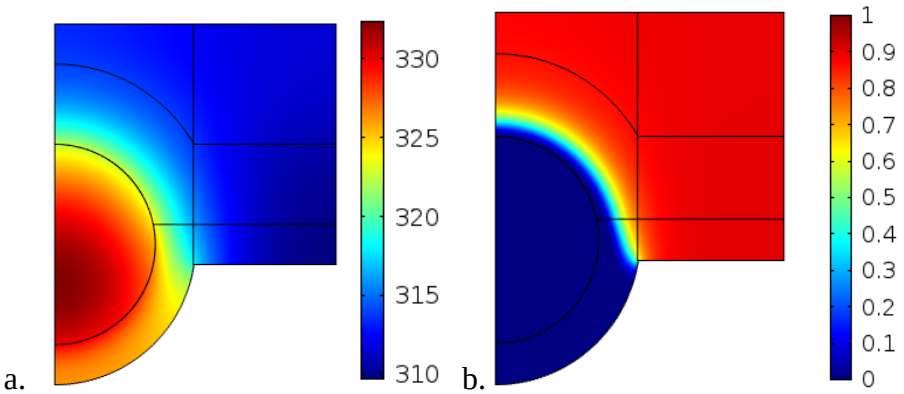

Figure 9. Model for the recommended treatment of 60 seconds of hyperthermia and 0.35 Gy of radiation treatment. (a) Temperature profile shows higher values towards the protrusion of the tumor. (b) Survival fraction profile shows lower values towards the protrusion of the tumor.

As seen in Figure 9, a majority of the 115 m^3 tumor is ablated with 60 seconds of heating with 1.5W/cm^2 infrared lamp followed by 0.35 Gy of radiation therapy. To understand how ambiguity in tissue parameters affected the results of the model, we performed a sensitivity analysis.

Sensitivity Analysis for Hyperthermia-Radiation

The linear quadratic model for survival fraction is dependent on four main parameters: dosage, fractionation, α, and β. Dosage is what we were solving for in the model. Fractionation is held constant at 1 (meaning the tumor is only irradiated once) to compare our results with known experimental results. It is also a controllable variable. α/β are cancer-dependent parameters that characterizes the radiation damage. Large α/β describes rapidly dividing tissue and α is more important in determining survival fraction [3]. Small α/β describes slowly proliferating tissue and β is more important in determining survival fraction [3]. Both α and β are expected to vary with temperature since hyperthermia sensitizes the tissue to radiation. Since SCC has an α/β of approximately 0.6 and it has been shown that β varies less with temperature, sensitivity analysis was performed on α. A parametric sweep for α was used and optimization functions for each were plotted. The best hyperthermia time for all the models was 60 seconds. The recommended dosages for each α was found and plotted against the α in Figure 10 below. The average survival fractions of the skin and the tumor were determined for the recommended dosages and also plotted in Figure 10.

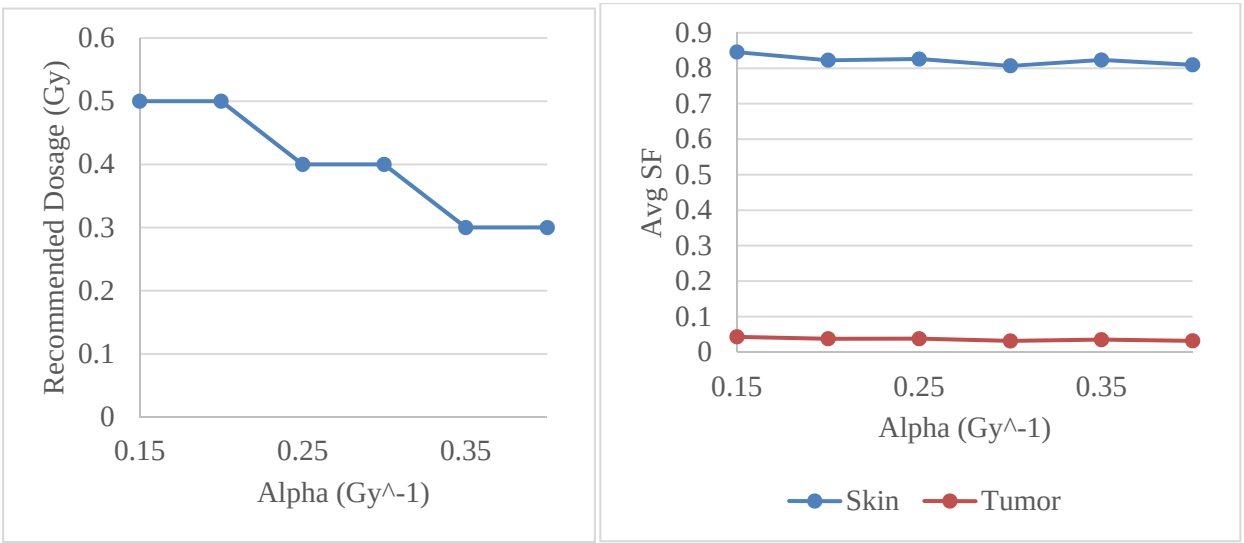

Figure 10. Sensitivity analysis for α in hyperthermia-radiation model. A parametric sweep was constructed for α and optimization for time-dosage was performed for each α to obtain recommended dosage (left). The recommendations were 0.4±0.1 Gy for α values 0.27±0.13 Gy^{-1}. The average survival fractions of the skin and of the tumor were determined for each of the recommended dosages (right). The average survival fraction ratio of skin:tumor was always approximately 0.83:0.03.

The results show that the recommended dosage for 115 mm^3 tumor hovered around 0.4±0.1 Gy when α ranged from 0.15-0.40 Gy^{-1}. This was 57% margin of error compared to the recommended 0.35 Gy recommended dosage with α=0.273 Gy^{-1}. The dosage showed variability, but the ratio of average survival fractions of skin:tumor for 60 seconds of hyperthermia and the recommended dosages was held relatively constant at approximately 0.83:0.03. Therefore, α ranging from 0.15-0.40 Gy^{-1} did not show much impact on the result.

The recommended treatment for a 115 mm^3 squamous cell carcinoma tumor located 1 mm below the epidermal surface in AuNP-hyperthermia-radiation therapy with a 1.5 W/cm^2 infrared lamp and AuNP injection of 100uL of 100mg/mL was determined to be 40 seconds of hyperthermia and 0.35 Gy of radiation. This result was achieved with an optimization function and the robustness of the recommended treatment was probed with a sensitivity analysis for the most uncertain parameter, α.

V. Discussion

Validation of AuNP Diffusion Profile and Experimental Studies

When AuNPs are injected into tissue, they are allowed to diffuse throughout the tumor. As shown in the sensitivity analysis, diffusivity of the AuNPs plays a crucial role in how far they spread. AuNPs have tunable properties, making them easily adaptable. Our diffusion model was validated by comparing our diffusion profile with experimental diffusion profiles. Hainfeld et al. did a qualitative analysis of the diffusion of the AuNPs after they were allowed to diffuse for 24 hours [2]. They found that the nanoparticles were primarily concentrated in the tumor and that they were aggregated here, as indicated by the black coloring in this region (Figure 11) [2]. They additionally found that the nanoparticles that did diffuse beyond the boundary of the tumor were red in color, indicating non-aggregated nanoparticles [2].

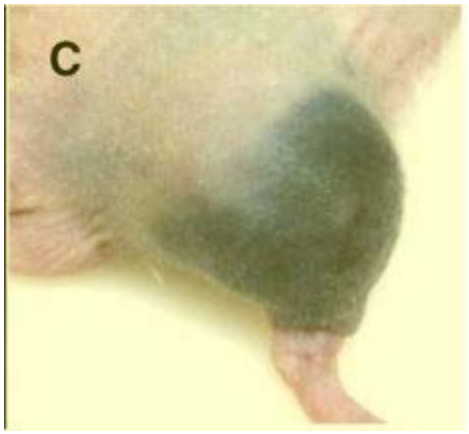

Figure 11. Image of tumor region after nanoparticle diffusion time of 24 hours. The darkening of the region indicates that nanoparticles are primarily concentrated, and also aggregated, in this region [2].

Validation of Hyperthermia Module

When AuNPs are injected into tissue, they demonstrate a significant increase in absorption in the infrared spectrum only they aggregate into clusters within cells. More AuNPs tend to aggregate in tumor cells than in healthy cells because of different extracellular conditions, and therefore cause drastic temperature differences when the two tissues are heated with infrared lamps.

When we modeled the hyperthermia process, we made several physical approximations for simplification. One of the major assumptions made was that *all* AuNPs aggregated into clusters within tumor cells and none aggregated within healthy tissue. Although this does not actually occur, the assumption allowed us to simplify unexplored kinetic properties involved with AuNP aggregation. Knowing this, we predicted that our final temperature values would be slightly overestimated for the tumor.

Validation for our hyperthermia model was approached in two ways. First, we compared the temperature profiles of tumors with AuNPs and tumors without AuNPs. Then we compared average temperatures from our model with experimental data in literature.

For our first approach, we disabled the infrared radiation term for the tumor and computed the temperature profile after 40 seconds. The result is shown in Figure 12 below.

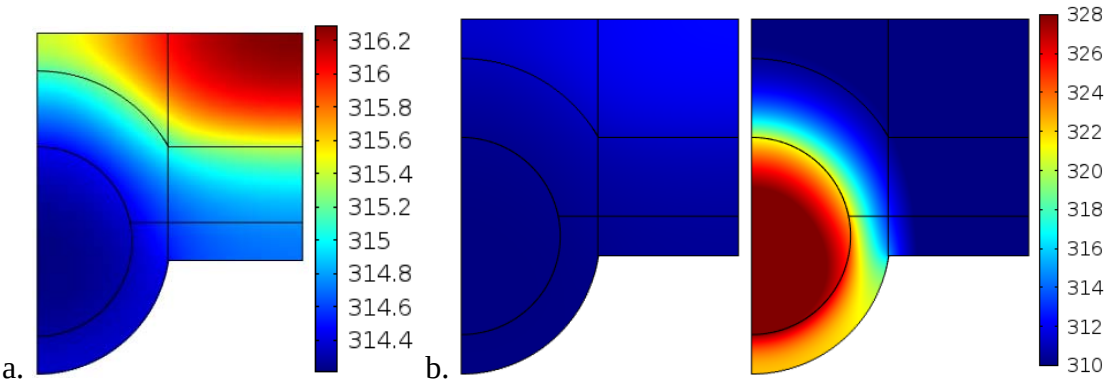

Figure 12. Temperature profiles of infrared therapy without AuNPs after 40 seconds of heating with a 1.5W/cm^2 lamp. (a) Most of the temperature is from metabolic heat generation in the tumor as expected. (b) Temperature profile of the tumor without AuNPs (left) is compared with the temperature profile of the tumor with AuNPs (right). There appears to be a significant 10°C increase in temperature around the tumor with AuNPs as expected.

We expected our tumor to be slightly warmer than surrounding tissue because of the tumor's relatively high metabolic heat generation from continuous proliferation. This was seen in Figure 12a. But we expect a tumor infused with AuNP to be higher than a tumor without AuNPs. This is shown in Figure 12b. However, we acknowledge that our model is limited. To a limited degree, normal tissue still absorbs infrared wavelengths. This was ignored in the governing equation proposed in Appendix A since AuNPs did not absorb infrared wavelengths in healthy tissue, making the term relatively negligible compared to the tumor's absorption in the infrared spectrum.

We then compared our hyperthermia results with known experimental data in Figure 13. After 40 seconds of heating with 1.5 W/cm^2 infrared lamp, the tumor in our hyperthermia model is 49.5°C, which has only a 3% error deviating from the experimental data 48°C [2].

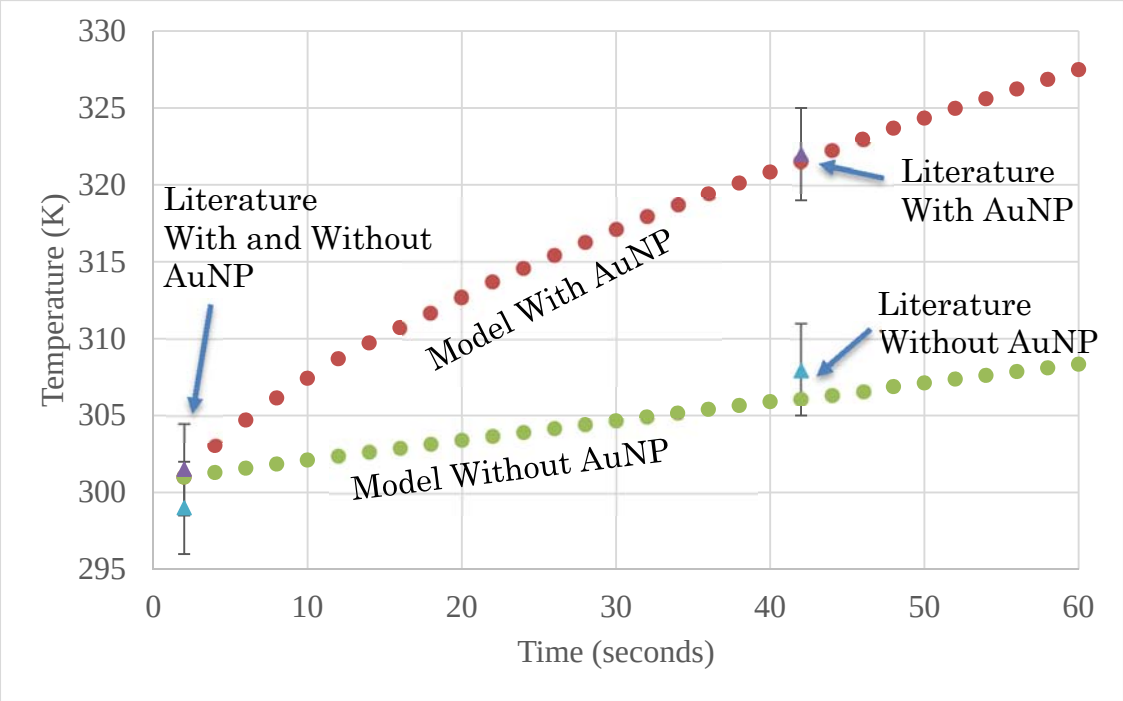

Figure 13. Comparison of hyperthermia model with experimental data from literature [2]. The model showed an average tumor temperature of 27°C at t=0s and of 48.5°C at t=40s. Both predicted temperatures lie within the margin of error range for experimentally measured data of 28±3°C and 48±3°C from Hainfeld, et. al.

Because we assumed perfect aggregation of AuNPs inside tumor cells and insulated the boundaries of the tumor-tissue model, we expected the model's temperature to overestimate the actual temperatures. However, for hyperthermia timelength less than 40 seconds, the model still appears to be accurate with these assumptions.

Validation of Hyperthermia-Radiation Modeling

AuNP mediated hyperthermia process has only recently been coupled with X-ray radiation therapy as a noninvasive method for cancer treatment. Therefore, there is a limited amount of experimental data available for validation of our model. However, there are trends in the survival curves of radiosensitive SCC lines and radioresistant SCC lines [16]. Since hyperthermia radiosensitizes the tumor cells to radiation therapy, we propose to compare the trends in hyperthermia with trends in radioresistance. Survival fraction curves were generated for both cases and compared to in Figure 14 below.

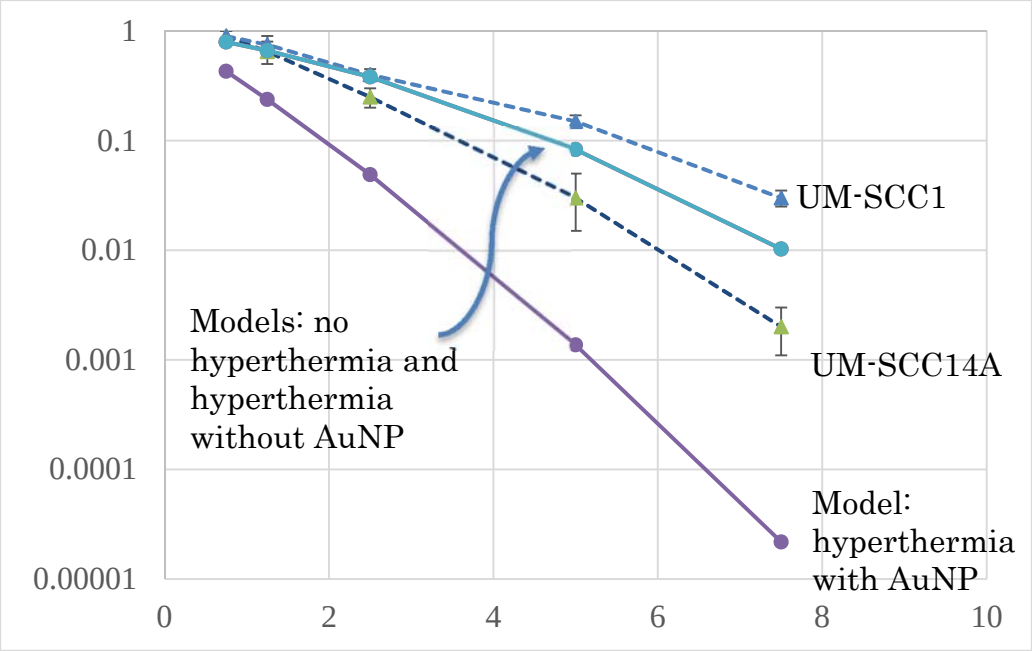

Figure 14. Survival curves comparing model results and experimental data from literature [16]. The dashed lines represent cell lines UM-SCC14A (a radiosensitive SCC line) and UM-SCC1 (a radioresistant SCC line). The experiments were in vitro: cells were grown on petri dishes. The solid lines represent the results from the hyperthermia-radiation model: (1) no hyperthermia, (2) hyperthermia without AuNP, and (3) hyperthermia with AuNP. Lines (1) and (2) falls on the same values. Hyperthermia treatments were modeled as 10 seconds of heating with a 1.5W/cm^2 infrared lamp.

UM-SCC1 and UM-SCC14A were SCC cell lines that were grown on petri dishes. They were radiated in vitro and the survival fractions were calculated by comparing the decreasing number of colonies remaining in the plates. UM-SCC1 is the radioresistant cell line and UM-SCC14A is the radiosensitive cell line. To compare our hyperthermia-radiation model to the experimental data's trends, we needed to modify our model. The cell lines were incubated at 37°C prior to radiation, so initial temperature was set to 37°C. We then generated three models: (1) radiation with no hyperthermia and no AuNP, (2) radiation with hyperthermia and no AuNP, and (3) radiation with hyperthermia and with AuNP. As we expected, the survival curve of our model with no hyperthermia and no AuNPs was in-between the curves for these two extreme cell lines. In addition, hyperthermia tend to shift the survival curve lower with increasing dosage, following the radiosensitized UMSCC14A curve as expected.

In the process of altering the initial conditions for validating our hyperthermia-radiation modeling, we noticed that lower initial temperatures could aid to how drastic the temperatures are. When the tissue started at 28°C in the initial phase of hyperthermia, the epidermis and dermis stay less than 43°C for a longer period of time. Furthermore, the survival fraction of

healthy tissue is slightly higher. We modeled the survival fraction of 28°C and of 37°C over the course of hyperthermia treatment. The results are shown below in Figure 15.

a.

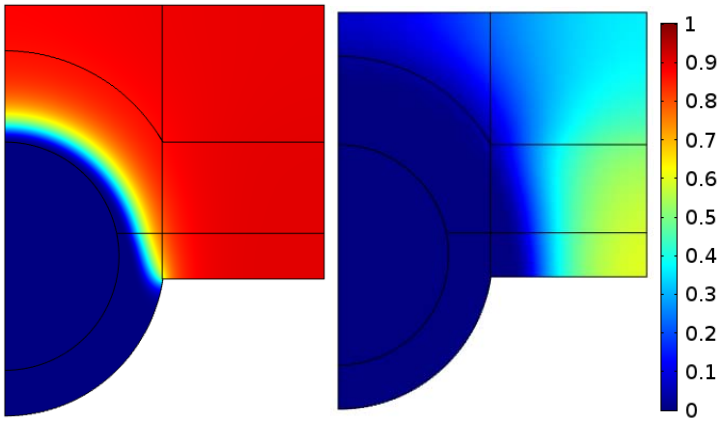

b.

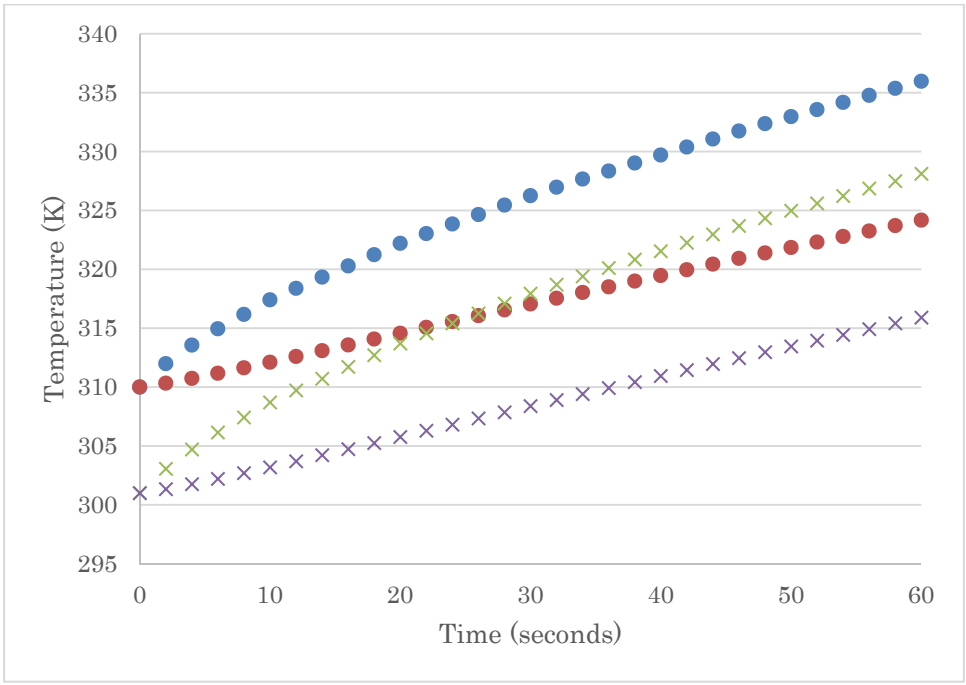

Figure 15. Survival fraction profile and average temperatures of tumor and healthy tissue at 28°C and at 37°C. (a) The left shows the survival fraction profile of the tissue at the recommended dosimetry when the initial temperature is 28°C and the right shows the survival fraction profile at 37°C. (b) The average temperatures are shown in the graph. If the initial temperature is lower, the healthy tissue could withstand 60 seconds of hyperthermia. If the initial temperature is higher, the healthy tissue could withstand 20 seconds of hyperthermia. Starting the tissue at lower temperatures would allow a greater temperature contrast for more effective radiation therapy.

Temperature profiles show a slightly larger difference of 12.2°C between the tumor and the healthy tissue when the initial temperature was at 28°C, compared to 11.8°C difference when the

initial temperature was at 37°C. This suggests that cooling the tissue before hyperthermia could further increase the control for radiation therapy.

VI. Conclusions

Our work indicates that computational modeling is a feasible option for modeling gold nanoparticle hyperthermia and radiation therapy for cutaneous squamous cell carcinoma, by utilizing linear-quadratic modeling numerical methods. Using this method, we were able to compute optimal hyperthermia time and radiation dosage such that tumor death was maximized, damage to healthy tissue was minimized, and radiation dosage was minimized. We determined that this optimal combination for our particular model is a hyperthermia treatment for 60 seconds, followed by a radiation dosage of 0.35 Gy. We are confident that with the availability of additional parameters, this model could be tailored to other types of cancers or tumor geometries.

Notably, we found that survival fraction of the healthy tissue increased when the initial temperature of the tissue prior to hyperthermia-radiation treatment was decreased. This is because AuNPs were allowed more time to absorb in the near infrared spectrum during the hyperthermia heating process before surrounding tissues would be at risk for irreversible damage. This suggests that an additional cooling step prior to hyperthermia would be an added step in the treatment process that could potentially give physicians greater control on tumor ablation, by allowing for greater tumor temperature increases with less damage to surrounding tissues.

An important avenue of future research is the mechanism of gold nanoparticle aggregation. A significant limitation of our model was that it assumed that all nanoparticles in the tumor aggregate. Based on our results, specifically the low optimal radiation dosage computed compared to experimental dosages, it is likely that only a small portion of the nanoparticles aggregate. Studying the chemical mechanism associated with this aggregation process would allow for the coupling of the diffusion and heat transfer models, which would significantly improve accuracy of the model.

Another future research direction is expanding the hyperthermia-radiation therapy model. The treatment process can be used to target other tumors that are localized nodules and within range of near infrared penetration depth. This would require alteration of the personalized hyperthermia-radiation treatment. Tumor resistance to radiotherapy varies from patient to patient, even within squamous cell carcinoma cell lines. Assessing the availability of parameters for other types of tumors utilizing this therapy, such as prostate cancer, could result in wide applicability of this modeling and optimization mechanism.

Appendix A: Problem Statement

Clinical use of consecutive hyperthermia and radiotherapy treatments is limited because of the unexplored hyperthermia time length and radiotherapy dosage combinations. Treatment has also been assumed to be viable after 24 hours of incubation. A model of AuNP diffusion and hyperthermia-radiation treatment would resolve ambiguities and aid the treatment process. Our project can be divided into three modules: diffusion of AuNPs, hyperthermia, and radiation.

Module 1 – Diffusion of Gold Nanoparticles

For the first part of the AuNP-hyperthermia-radiation therapy, nanoparticles are injected at a constant rate directly into the tumor using a syringe. They are then allowed to diffuse throughout the tumor before hyperthermia to ensure even heating of the tumor. In literature, researchers assumed a 24 hour waiting period for even nanoparticles diffusion. With this module, we want to determine the shortest waiting period between the AuNP injection and hyperthermia processes and confirm the even distribution of nanoparticles.

Governing Equations:

The diffusion of AuNPs is modeled using the mass species governing equation with a transient term, a diffusion term, and a generation term. It is assumed that there is no convection and degradation for the nanoparticles.

$$\frac{\partial c}{\partial t} = D_{AB}\left(\frac{1}{r}\frac{\partial}{\partial r}\left(r\frac{\partial c}{\partial r}\right) + \frac{\partial^2 c}{\partial z^2}\right) + R_{INJ} \tag{A1}$$

The generation term is present within the center of the tumor for to model the injection of nanoparticles. The rate of injection was 4uL/min with 100uL of 100 mg AuNP/mL. This was modeled with the equation below:

$$R_{INJ} = \frac{\frac{.1\ mL}{min}\cdot\frac{1\ min}{60\ sec}\cdot\frac{100\ mg\ AuNP}{mL}}{V_{INJ}} \tag{A2}$$

Where V_{INJ} is the volume of the injection site, determined using and integration function on COMSOL.

Boundary and Initial Conditions:

It is assumed the patient has no AuNP in the system prior to injection. So the initial condition is true in all domains.

$$c|_{t=0} = 0 \tag{A3}$$

The purpose of the module is to monitoring the diffusion of the nanoparticles until it is evenly distributed within only the tumor region. Boundaries 1-3 and 5 are considered far from the region of interest, so they were set to have a zero flux boundary equation. After running the simulation, we saw that nanoparticles did not diffuse much through the healthy tissue and there were no nanoparticles at the boundaries. So, we kept the zero flux boundary equations. Boundary 4 also has a zero flux boundary equation due to symmetry.

$$\left.\frac{\partial c}{\partial x}\right|_{B1-5} = 0 \tag{A4}$$

Module 2 – Hyperthermia

For the second part of the AuNP-hyperthermia-radiation therapy, the tumor is heated using near infrared spectrum. A halogen lamp and a 780 nm high pass filter is used to heat the tumor at 1.5 W/cm^2. After the tumor has been heated to 48°C, researchers have delivered different dosages of X ray irradiation and monitored the tumor shrinkage over time. With this module, we will simulate the heating of tumor and surrounding healthy tissue using the near infrared spectrum and then use the resulting tumor and tissue temperatures to determine their respective survival fractions.

Governing Equation:

Hyperthermia is modeled using the heat governing equation with a transient term, a heat diffusion term, a blood perfusion term, a tumor metabolic generation term, and a heat generation term from absorption of the near infrared spectrum.

$$\rho_t C_t \frac{\partial T}{\partial t} = k_t \left[\frac{1}{r}\frac{\partial}{\partial r}\left(r\frac{\partial T}{\partial r}\right) + \frac{\partial^2 T}{\partial z^2}\right] + V\rho_b C_b (T_b - T) + Q_m + Q_{IR} \tag{A5}$$

Within the tumor region, nanoparticles aggregate and can absorb at the 700nm-1000nm region. Beyond the tumor region, nanoparticles do not aggregate and there is a negligible amount of absorbance. Therefore, the heat generation term for near infrared absorbance is employed only within the tumor region. This absorption decays with respect to depth and is modeled as follows

$$Q = Q_0 e^{\left(\frac{-z}{\delta}\right)} \tag{A6}$$

The penetration depth of infrared spectrum is approximately 35mm. With a 1.5Wcm^{-2} lamp shining perpendicular to the skin, that would give the following equation

$$Q_{IR} = \frac{0.015 W mm^{-2}}{35mm} e^{\left(\frac{-(z-z_0)}{35mm}\right)} \tag{A7}$$

where z is the depth and z_0 is the surface of the epidermis. The metabolic heat generation of the tumor was found using the tumor heat generation equation, where τ is the doubling time of the tumor [6].

$$Q_m\tau = 3.27 * 10^6 \ \frac{W}{m^3} \cdot days \tag{A8}$$

Boundary and Initial Conditions:
Hyperthermia is a short process. For simplification of the model, we used a zero-flux equation for Boundaries 1-3.

$$k\frac{\partial T}{\partial r} = 0 \tag{A9}$$

Boundary 4 reflects the axis symmetry.

$$\left.\frac{\partial T}{\partial r}\right|_{r=0} = 0 \tag{A10}$$

Boundary 5 is where the skin is exposed to the infrared heat source, but the term is incorporated as a heat generation term in the governing equation. Assuming negligible convection during this short time frame, we set this boundary to a zero-flux equation.

The tissue before heating is set as the initial temperature found in the procedure as described in Hainfield, et. al.'s experimental paper.

$$T|_{t=0} = 300\ K \tag{A11}$$

Module 3 – Radiation Dosages
For optimization, we need to relate survival fraction, radiation dosage, and heating duration. The equation used to model radiation therapy for tumor treatment is

$$SF = \exp[-d\left(\alpha + \frac{\beta d}{n}\right)] \tag{A12}$$

where SF is survival, d is the dosage level, n is the number of short-fraction irradiation, and α and β are tumor-specific parameters fitted into the Poisson distribution. For SCC treatment with a single fraction, α=0.273Gy^{-1} and β=0.045Gy^{-2} at

$$d_{HT} = \frac{-\alpha+\sqrt{\alpha^2+4\beta d(\alpha(T)+d\beta(T))}}{2\beta} \tag{A13}$$

where d_{HT} is the dosage equivalent for hyperthermia to yield a similar therapeutic effect as the conventional dose with equivalent tumor control probability.

$$\alpha_{exp}(T) = \alpha_{37} e^{(T-37)^2/T_0}, T_0 = \frac{16}{ln\frac{\alpha_{lin}(41)}{\alpha_{37}}} \tag{A14}$$

such that

$$a_{lin}(T) = \alpha_{37} + \frac{1.5\alpha_{37} - \alpha_{37}}{41-37}(T - 37) \tag{A15}$$

Input Parameters

Parameters drawn from multiple sources were used to describe both the AuNP diffusion process and the hyperthermia process and are listed in Table 1 below.

Table 1: Input parameters used in the model

Input Parameter	Value
Tumor Doubling Time (τ) [8]	131 days
Tumor Volume [2]	115 mm^3
Specific Heat Capacity of Tumor (c_T) [4]	3639 $\frac{J}{kg \cdot K}$
Thermal Conductivity of Tumor (k_T) [4]	0.56 $\frac{W}{m \cdot K}$
Density of Tumor (ρ_T) [4]	1050 $\frac{kg}{m^3}$
Blood Perfusion of Tumor (V_{Tb}) [4]	$5.0*10^{-3}$ $\frac{m^3{}_{blood}}{m^3{}_{tissue} \cdot s}$
Specific Heat Capacity of Epidermis (c_E) [9]	3182 $\frac{J}{kg \cdot K}$
Thermal Conductivity of Epidermis (k_E) [10]	0.21 $\frac{W}{m \cdot K}$
Density of Epidermis (ρ_E) [10]	1050 $\frac{kg}{m^3}$
Blood Perfusion of Epidermis (V_{Eb}) [10]	0 $\frac{m^3{}_{\square lood}}{m^3{}_{tissue} \cdot s}$
Metabolic Heat Generation of Epidermis (Q_{ME}) [11]	0 $\frac{W}{m^3}$
Specific Heat Capacity of Dermis (c_D) [9]	2846 $\frac{J}{kg \cdot K}$
Thermal Conductivity of Dermis (k_D) [10]	0.30 $\frac{W}{m \cdot K}$
Density of Dermis (ρ_D) [10]	1050 $\frac{kg}{m^3}$
Blood Perfusion of Dermis (V_{Eb}) [10]	$1.63*10^{-3}$ $\frac{m^3{}_{blood}}{m^3{}_{tissue} \cdot s}$
Metabolic Heat Generation of Dermis (Q_{MD}) [11]	627.8 $\frac{W}{m^3}$
Specific Heat Capacity of Subcutaneous Fat (c_S) [4]	2387 $\frac{J}{kg \cdot K}$
Thermal Conductivity of Subcutaneous Fat (k_S) [4]	0.22 $\frac{W}{m \cdot K}$
Density of Subcutaneous Fat (ρ_S) [4]	888 $\frac{kg}{m^3}$
Blood Perfusion of Subcutaneous Fat (V_{Sb}) [10]	$1.0*10^{-3}$ $\frac{m^3{}_{blood}}{m^3{}_{tissue} \cdot s}$
Metabolic Heat Generation of Subcutaneous Fat (Q_S) [11]	$3.767*10^{3}$ $\frac{W}{m^3}$
Diffusivity of AuNP in Tumor [12]	$9.0*10^{-11}$ $\frac{m^2}{s}$

Diffusivity of AuNP in Tissue [12]	$9.0*10^{-12}\ \frac{m^2}{s}$

This table contains the physical and chemical properties used in this model. The dimensions for the tumor are also labeled in the schematics shown on Page 7.

Appendix B: Solution Strategy

The tumor ablation process was broken down into three modules: AuNP diffusion, hyperthermia, and radiation, as shown in Figure B1.

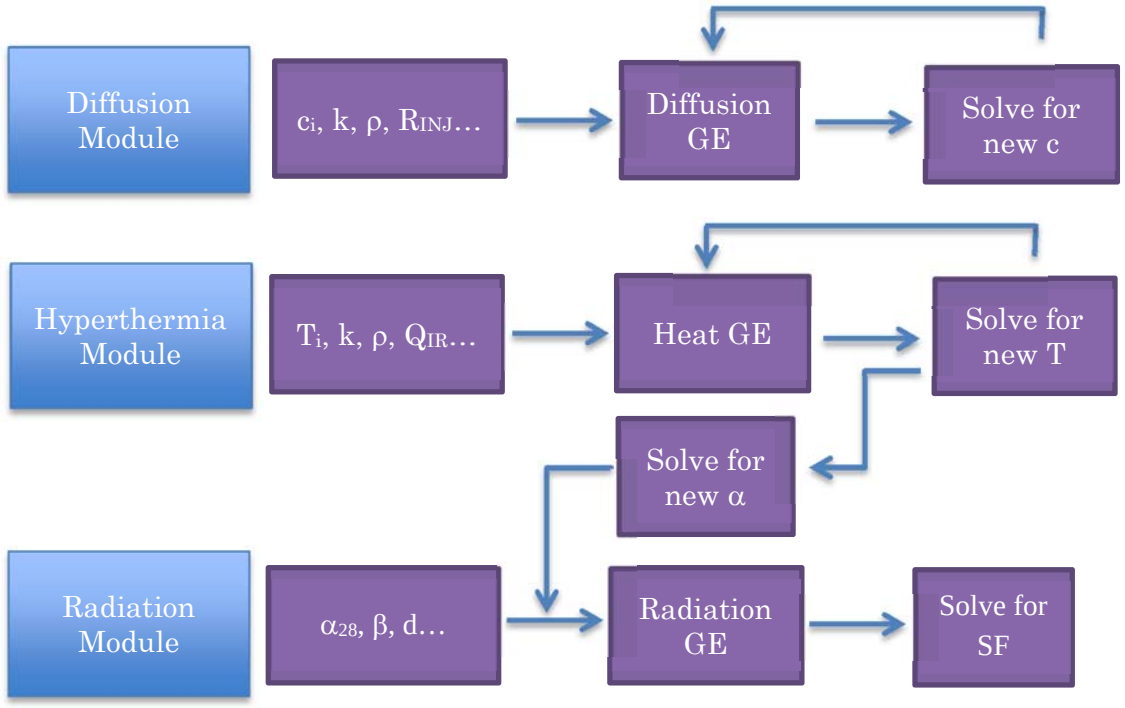

Figure B1. Schematic of solution strategy. Diffusion module was solved standalone, but was necessary to confirm assumptions made for the hyperthermia module. Hyperthermia module was necessary to be solved to determine changing α parameters that were used in the radiation module.

AuNP diffusion module was solved stand-alone while results from the hyperthermia module were fed into the radiation module. All modules were solved using the default PARDISO linear solver. The time and mesh convergences for AuNP diffusion and hyperthermia are described below.

Module 1 – Diffusion of Gold Nanoparticles

Time Convergence Analysis

Time convergence analysis was performed by analyzing the temperature convergence at 2D cutpoint (0.0035m, 0.0025m) after 24 hours of diffusion. This 2D cut point was chosen due to its significance a boundary point between the tumor and the surrounding tissue. Figure B2 shows convergence at a time step of around 500 seconds. Since computation time was not an issue for this model, a time step of 10 seconds was used for the actual modeling process.

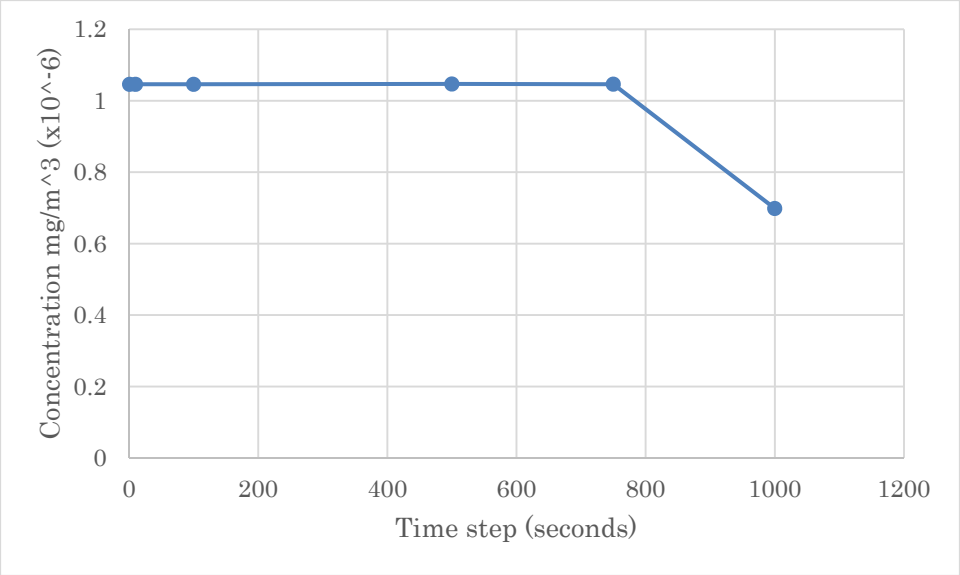

Figure B2. Time convergence analysis for diffusion of AuNPs at 2D cutpoint (0.0035m, 0.0025m) at t = 24hrs.

Mesh Convergence Analysis

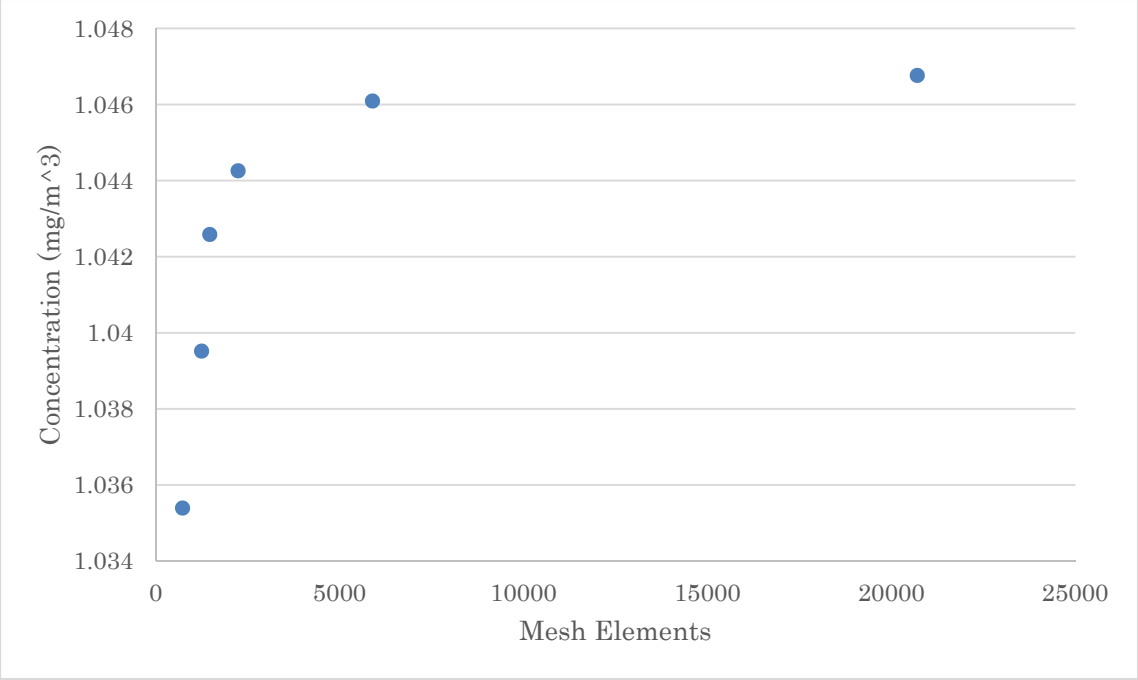

Figure B3. Mesh convergence analysis for modeling AuNP diffusion at 2D cutpoint (0.0035, 0.0025) at t=24 hr. The plot shows that the concentration of AuNPs converge to 1.047 mg/m^3 around 10,000 mesh elements.

A free triangular mesh was created and a mesh convergence analysis was performed for the diffusion model. The mesh convergence analysis was performed by analyzing the

concentration at 2D cut point (0.0035, 0.0025) because of this point's significance of being located on the interface between the tumor and the surrounding tissue. Total number of mesh elements was varied from 1000 to 20,000 elements. The mesh converged neatly at 10,000 elements, which corresponds to COMSOL's fine mesh setting.

Module 2 – Hyperthermia

Time Convergence Analysis

Time convergence analysis was performed by analyzing the temperature convergence at 2D cutpoint (0.0035m, 0.0025m) after 60 seconds of heating. This cutpoint was chosen at the tumor-tissue interface because it was expected to have the largest temperature gradient since the AuNPs absorb infrared energy in the tumor and the AuNPs do not in the healthy tissue. The time analyzed was chosen because radiation therapy is usually performed for a short period of time clinically. A parametric sweep was used with varying time-steps (0, 2, 4, 6, 10, 15, and 30 seconds) and the temperatures at the cutpoint are plotted in Figure B4.

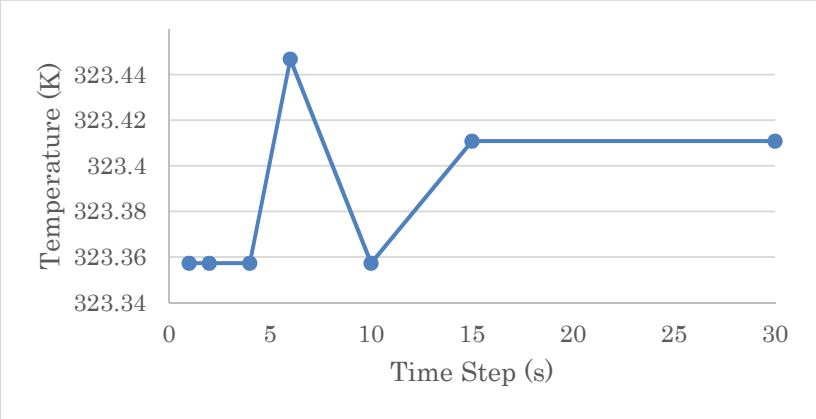

Figure B4. Time convergence analysis for hyperthermia model at 2D cutpoint (0.0035m, 0.0025m) at t = 60s. The temperature appears to be steady around 323.36 K when the timestep is smaller than 4s.

The temperature appears to be steady around 323.36 K when the time-step is smaller than 4 seconds. However, since the model was not limited in computational time, we decided to use a time-step for 2 seconds for our computations.

Mesh Convergence Analysis

Mesh convergence analysis was performed for thermal heating modeling in hyperthermia. The temperature was analyzed also at (0.0035m, 0.0025m) at the tumor/healthy-tissue interface using free triangular mesh. The first analysis was performed by varying the number of mesh points along the tumor-tissue interface. The result is shown in Figure B5a below. The axis for the graph is already narrow with a range of 0.14K, but the temperature stabilized around 323.58K beyond 150 total mesh points. This distribution of mesh points was held constant for our second analysis,

in which the total number of mesh elements throughout the model was allowed to vary. The temperature was again analyzed at (0.0035m, 0.0025m). The results are shown in Figure B5b below.

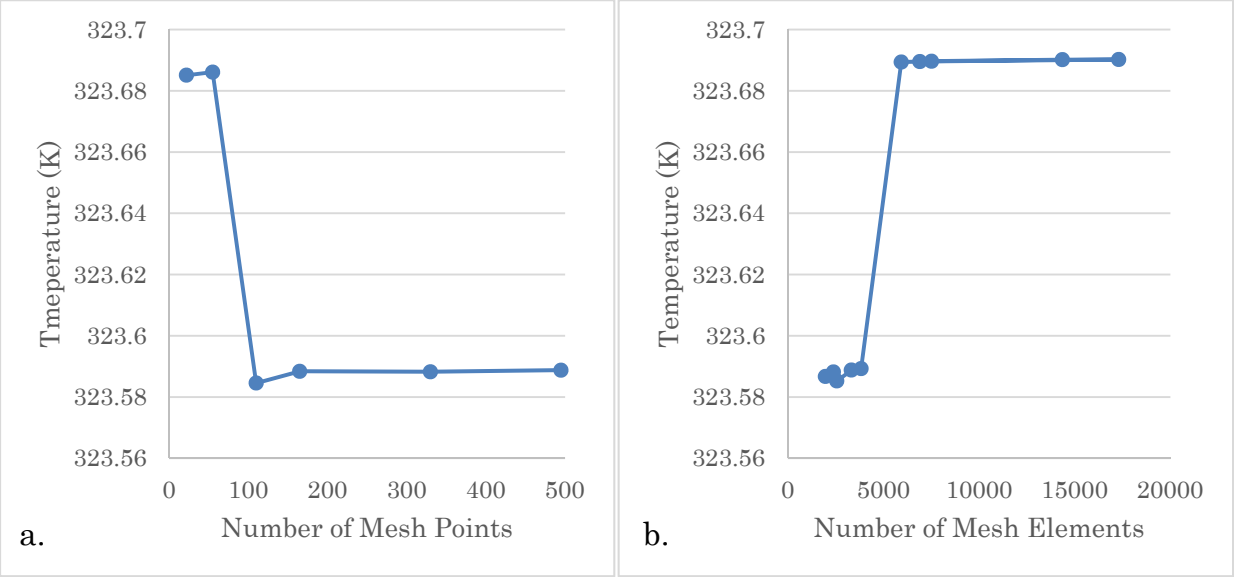

Figure B5. Mesh convergence analysis for modeling hyperthermia at 2D cutpoint (0.0035, 0.0025) at t=60s. (a, left) The plot shows that the temperature stabilizes at approximately 323.58K after 150 total meshes points. (b, right) The plot shows that the temperature stabilizes at approximately 346.48K beyond 5000 mesh elements.

The temperatures collected for this parametric sweep was also within 0.14 K, but the temperature seemed to stabilize around 323.69 K beyond 5000 mesh elements. We used these configurations and developed the mesh shown in Figure B6.

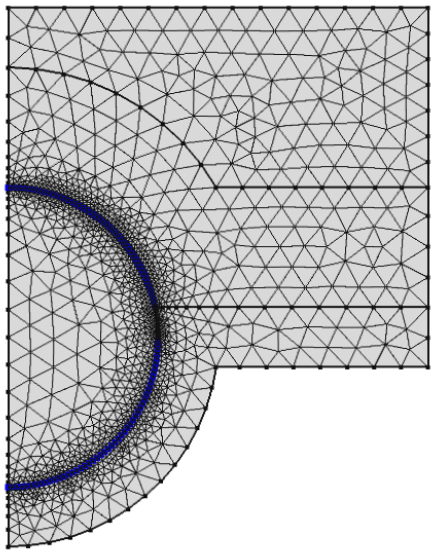

Figure B6. Mesh used for hyperthermia module. At the tumor-tissue interface, 150 mesh points were used. A total of 5000 mesh elements were used throughout the model.

The hyperthermia models were solved using the default PARDISO linear solver for all the modules. Transient processes were modeled with a time-step of 2 seconds from 0-60 seconds of hyperthermia, and spatial calculations were modeled with 5000 mesh elements with 150 mesh.

Module 3 – Radiation

Radiation was not modeled in COMSOL. We used the temperature profiles created from the hyperthermia model and coupled the result with modified linear quadratic equations found in Appendix A.

References

[1] 11 November 2011. [Online]. Available: http://www.nanotech-now.com/news.cgi?story_id=43849.

[2] J. Hainfeld, L. Lin, D. Slatkin, F. Dilmanian, T. Vadas and H. Smilowitz, "Gold nanoparticle hyperthermia reduces radiotherapy dose," *Nanotechnology, Biology, and Medicine,* vol. 10, pp. 1609-1617, 2014.

[3] V. Yanofsky, S. Mercer and R. Phelps, "Histopathological Variants of Cutaneous Squamous Cell Carcinoma: A Review," *Journal of Skin Cancer,* vol. Volume 2011, pp. 1-13, 2011.

[4] H. Kok, J. Crezee, N. S. L. Franken, G. Barendsen and A. Bel, "Quantifying the Combined Effect of Radiation Therapy and Hyperthermia in Terms of Equivalent Dose Distributions," *International Journal of Radiation Oncology*Biology*Physics,* vol. 88, pp. 739-735, 2013.

[5] E. Jones, O. J., L. Prosnitz, T. Samulski, Z. Vuiaskovic, D. S. L. Yu and M. Dewhirst, "Randomized Trial of Hyperthermia and Radiation for Superficial Tumors," *Journal of Clinical Oncology,* vol. 13, no. 1, pp. 3079-3085, 2005.

[6] L. C. Kennedy, L. R. Bickford, N. A. Lewinski, A. J. Coughlin, Y. Hu, E. S. Day, J. L. West and R. A. Dresek, "A New Era For Cancer Treatment: Gold-Nanoparticle-Mediated Thermal Therapies," *Small,* vol. 7, no. 2, pp. 169-183, 2011.

[7] R. Grenman, D. Burk, E. Virolainen, J. G. Wagner, A. S. Lichter and T. E. Carey, "Radiosensitivity of Head and Neck Cancer Cells In Vitro," *Arch Otolaryngol Head Neck Surg,* vol. 114, 1988.

[8] R. Wilkins and G. Wilkins, Neurosurgical classics II, Park Ridge, Illinois: American Assoiciation of Neurological Surgeons, 2000.

[9] A. Datta and V. Rakesh, An introduction to modeling of transport processes: applications to biomedical systems, Cambridge, UK: Cambridge University Press, 2010.

[10] J. Jiao and Z. Guo, "Thermal interaction of short-pulsed laser focused beams with skin tissues," *Physics in Medicine and Biology,* vol. 54, pp. 4225-4241, 2009.

[11] D. Gurung, "Two dimensional temperature distibution model in human dermal region exposed at low ambient temperatures with air flow," *Kathmandu University Journal of Science, Engineering and Technology,* vol. 8, no. II, pp. 11-24, 2012.

[12] D. Brenner, "The Linear-Quadratic Model Is an Appropriate Methodology for Determining Isoeffective Doses at Large Doses Per Fraction," *Seminars in Radiation Oncology,* vol. 18, no. 4, pp. 234-239, 2008.

[13] R. J. Yaes, "Some Implications of the Linear Quadratic Model for Tumor Control Probability," *Int J. Radiation Oncology Bio. Phys. ,* pp. 147-157, 14.

[14] S. O'Rourke, H. McAneney and T. Hillen, "Linear quadratic and tumour control probability modelling in external beam radiotherapy," *J. Math. Biol,* vol. 58, pp. 799-817, 2009.

[15] J. F. Hainfeld, M. O'Connor, P. Lin, L. Qian, D. N. Slatkin and H. M. Smilowitz, "Infrared-Transparent Gold Nanoparticles Converted by Tumors to Infrared Absorbers Cure Tumors in Mice by Photothermal Therapy," *Plos One,* vol. 9, no. 2, pp. 1-11, 2014.

[16] B. Kim, G. Han, B. J. Toley, C. Kim, V. M. Rotello and N. S. Forbes, "Tuning payload delivery in tumour cylindroids using gold nanoparticles," *Nature Nanotechnology,* vol. 5, pp. 465-472, 2010.

[17] G. Reidar, D. Burk, E. Virolainen, J. Wagner, A. LIchter and T. Carey, "Radiosensitivity of Head and Neck Cancer Cells In Vitro," *Arch Otharyngol Head Neck Surg,* vol. 114, pp. 427-431, April 1988